Int J Pept Res Ther (2009) 15:49–59
DOI 10.1007/s10989-008-9163-y

Binding and Uptake of RGD-Containing Ligands to Cellular $\alpha_v\beta_3$ Integrins

Sonya Cressman · Ying Sun · E. Jane Maxwell · Ning Fang · David D. Y. Chen · Pieter R. Cullis

Accepted: 17 November 2008 / Published online: 2 December 2008

Abstract The cyclic peptide, cRGDf[N(me)]V, binds to the $\alpha_v\beta_3$ integrin and can disrupt binding of the integrin to its natural ligands in the extracellular matrix. In this work, the ability of a water-soluble, fluorescently labeled variant of the RGD-containing peptide (cRGDfK-488) to bind to integrins on human umbilical vascular endothelial cells (HUVEC) and subsequently undergo endocytosis was characterized. This information was compared to the binding and uptake properties of an $\alpha_v\beta_3$ integrin-specific monoclonal antibody, LM609X. The specificity of the RGD-containing peptide is assessed by comparison with control peptide that does not bind to the $\alpha_v\beta_3$ integrin, cRADfK-488. Using a high purity construct, it is shown that the RGD ligand exhibits dissociation constants in the micromolar range whereas LM609X exhibits dissociation constants in the nanomolar range. However, the RGD ligand showed greater uptake following incubation at temperatures which permit endocytosis. A 7.4-fold increase in uptake of the RGD peptide was observed following a 1 h incubation with HUVEC at 37°C (an endocytosis permissive temperature), as compared to that at 4°C (an endocytosis prohibitive temperature). In contrast, only a 1.9-fold increase in cell-associated fluorescence was observed for similar incubations with LM609X. Results from fluorescence microscopy supports the notion that the RGD peptide is rapidly endocytosed at 37°C as compared to LM609X. These results are discussed with regard to previous work indicating that RGD ligands enter cells by integrin-independent pathways. These studies provide well-controlled measures of how RGD ligands stimulate endocytosis. This may be of considerable interest for intracellular delivery of ligand-associated drugs in anti-angiogenic applications.

Keywords $\alpha_v\beta_3$ integrins · RGD · Endocytosis · Angiogenesis

S. Cressman (✉) · P. R. Cullis
Department of Biochemistry, University of British Columbia, Vancouver, BC, Canada
e-mail: sonyacressman@hotmail.com

Y. Sun · E. J. Maxwell · N. Fang · D. D. Y. Chen
Department of Chemistry, University of British Columbia, Vancouver, BC, Canada

Introduction

Integrins are transmembrane proteins that mediate cell–cell interactions as well as interactions between cells and the extracellular matrix. The $\alpha_v\beta_3$ integrins have become important targets in the development of new anticancer strategies as they are expressed at high levels on the surface of many cancer cells (e.g., gliomas Gladson and Cheresh 1991, melanomas Albelda et al. 1990, ovarian carcinomas Liapis et al. 1997) as well as tumor-associated endothelial cells (Brooks et al. 1994). In addition, the $\alpha_v\beta_3$ integrins are involved in angiogenesis (Brooks et al. 1994), metastasis (Hieken et al. 1996) and resistance to radiotherapy (Albert et al. 2006; Smith and Giorgio 2004). The $\alpha_v\beta_3$ integrins on tumour-associated endothelial cells are considered to be particularly important targets given that all tumors require a blood supply for survival (Folkman 1990).

The wide variety of natural ligands for the $\alpha_v\beta_3$ integrins (e.g., vitronectin, fibronectin, osteopontin, denatured/proteolysed collagen and the foot and mouth disease virus) bind to the integrin by a conserved RGD tripeptide motif that is usually located on a flexible loop that extends out from the protein (Ruoslahti and Pierschbacher 1987). RGD-containing peptides antagonize the $\alpha_v\beta_3$ integrin and

have anti-angiogenic activity both in vitro (Brassard et al. 1999) and in vivo (Storgard et al. 1999). They are also thought to mimic structural features at the binding site of the natural integrin ligands. Kessler and colleagues have investigated in detail the binding sites between the peptide and the integrin that are responsible for anti-adhesive activity (Haubner et al. 1996), leading to the development of cRGDf[N(me)]V, a specific $\alpha_v\beta_3$ antagonist that is currently pursued as an anti-angiogenic drug candidate, known as Cilengitide™ (Dechantsreiter et al. 1999). A single substitution of glycine with alanine renders the RAD-containing peptides inactive, thus the equivalent RAD-containing peptides are a strong negative control for investigating the biological activity mediated by the $\alpha_v\beta_3$ integrin. Kessler and colleagues also demonstrate that Cilengitide™ and similar versions of Cilengitide™ (cRGDfK-) have negligible affinity for non-$\alpha_v\beta_3$ integrins, making these peptides ideal for the study of $\alpha_v\beta_3$ binding mechanisms (Pfaff et al. 1994).

Conjugates of Cilengitide™-like peptides (typically pentapeptides cyclized by disulphide linkages or more commonly by head-to-tail condensation) have also been used to target drugs (Arap et al. 1998; Burkhart et al. 2004; Kim and Lee 2004; Chen et al. 2005), antibodies (Schraa et al. 2004), imaging agents (von Wallbrunn et al. 2006; Montet et al. 2006b; Beer et al. 2006) and liposome encapsulated drugs (Dubey et al. 2004; Schiffelers et al. 2003; Xiong et al. 2005) to tumor sites. Improved drug delivery has been achieved when the targeting ligand is displayed in a multivalent form, a strategy also used by viruses and antibodies. When radionuclides are conjugated with dimeric (Chen et al. 2005) or (even better) tetrameric (Wu et al. 2005) RGD-containing peptides, localization to the site of a tumor is greatly enhanced. However, because of the complexity of their biology, the response of integrins to even monomeric RGD ligands remains poorly understood (Puklin-Faucher et al. 2006). This applies particularly to basic aspects such as endocytosis following binding of RGD ligands to integrins, where some reports suggest that binding does not lead to endocytosis (Castel et al. 2001) and others assume that binding is accompanied by endocytosis (Balasubramanian and Kuppuswamy 2003).

In this work we develop a highly purified and water-soluble, fluorescently labeled version of Cilengitide™, cRGDfK-488, and employ this ligand to investigate binding and subsequent endocytosis of RGD ligands to $\alpha_v\beta_3$ integrins, which are highly expressed on HUVECs. It is shown that the cRGDfK-488 is accumulated into HUVEC in a manner that is consistent with binding to the integrin receptor and subsequent endocytosis. Further, it is shown that the rate of endocytosis promoted by the presence of the RGD ligand is considerably greater than may be achieved by monoclonal antibodies against the integrin, a feature that supports the use of RGD peptides for enhancing intracellular delivery of ligand-associated drugs.

Materials and Methods

Materials

Unless specified, all reagents were obtained from Aldrich (Milwaukee, WI). Peptides were synthesized using 9-fluorenylmethyloxycarbonyl (FMOC) protected amino acids and resins obtained from EMD Biosciences (San Diego, CA), and dimethylformamide (DMF) as the main solvent. All solvents, of reagent grade or higher, were obtained from Fisher Scientific (Nepean, ON, Canada).

Reversed phase-high pressure liquid chromatography (RP-HPLC) was performed using gradients of aqueous acetonitrile (aqACN) containing 0.1% trifluoroacetic acid (TFA) on C18 columns purchased from Grace Vydac (Hesperia, CA). Analytical gradients were applied using column # 218TP5415 (dimensions 150 mm × 4.6 mm) with a flow rate of 1 ml per minute. All peptides were purified on a semi-preparative column (column # 218TP510, 250 mm × 10 mm) at a flow rate of 3 ml per minute.

Peptide Synthesis, Cyclization and Labeling

The linear sequences D(*t*-Bu)fK(Z)R(Pbf)G (the RGD-containing peptide) or D(*t*-Bu)fK(Z)R(Pbf)A (the control, alanine-containing peptide) were synthesized by FMOC-based solid phase peptide synthesis according to established methods. Briefly, peptides were assembled on 0.5 mM of 2-chlorotrityl resin using 1.3 molar equivalents (to carboxylic acid) of the following activating agents: *O*-benzotriazole-*N*,*N*,*N*′,*N*′-tetramethyl-uronium-hexafluorophosphate (HBTU) (Advanced Chemtech, Louisville, KT) and *N*-hydroxybenzotriazole (HOBT) (Advanced Chemtech, Louisville, KT) HOBT and HBTU. Peptides were activated in situ with triethylamine (TEA) then coupled to the resin for at least 1 h. FMOC removal steps were performed upon each amino acid addition by soaking the resin in a solution of 20% piperidine in DMF for 5 min, and repeated once. Between each step, the resin was washed with a constant flow of DMF for at least 1 min. Linear peptides were cleaved in 0.1% TFA in dichloromethane (DCM) with 2.5% triisopropyl silane (TIS) and H_2O (v/v). The crude peptide was analyzed by RP-HLPC with a linear gradient of 30–90% aqACN over 30 min (retention time 6.3 min) and by electrospray mass spectrometry (ESI–MS).

Lyophilized linear peptides were cyclized at 0.5 mM concentrations in DMF using benzotriazol-1-yl-oxytripyrrolidinophosphonium hexafluorophosphate (PyBop) and

HOBT to produce cR(Pbf)GD(*t*-Bu)fK(Z) or cR(Pbf)AD(*t*-Bu)fK(Z). Cyclization yields were typically over 95% and occurred within 30 min as indicated by RP-HPLC, with a retention time of 19.5 min on the same gradient as the linear peptide and a mass difference of 18 Da in the observed MW as measured by ESI–MS. ^{1}H NMR NOE assignments for all α-amide bonds confirmed a head-to-tail cyclic compound.

The lysine side chain was deprotected by hydrogenation with a palladium over carbon catalyst. The resulting compound (cR(Pbf)GD(*t*-Bu)fK or cR(Pbf)AD(*t*-Bu)fK) eluted at 11 min using the same RP-HPLC gradient as for the fully protected peptide. Conjugation of the cyclized RGD peptide to the Alexa Fluor-488 pentafluorophenol ester (Invitrogen, Carlesbad, CA) was performed in DMF, with the pH adjusted to 7.2 with TEA, and RP-HPLC purification was repeated using the same conditions as for the non-labelled peptide (Scheme 1).

Deprotection of the arginine and aspartic acid side chains was performed using a solution of 95% aqueous TFA and the reaction was subsequently purified by RP-HPLC with a gradient between 0 and 65% aqACN over 60 min. Both cRADfK-488 and cRGDfK-488 eluted at 19.5 min.

All peptides exhibited >95% purity as determined by capillary electrophoresis (CE). Product identification was validated by ESI–MS as follows: cRGDfK-488 (observed MW 1120.6; calculated MW 1120.1) and cRADfK-488 (observed MW 1134.2, calculated MW 1134.3). Peptides were lyophilized, weighed, and a standard curve for peptide quantification was established using the absorbance peak areas from chromatograms collected at 214 nm for peaks eluting between 12 and 13 min on a 0–65% AqACN analytical gradient over 30 min for the Alexa Fluor-488 labeled peptides. Typically, a 0.5 mM scale synthesis would yield 450 mg of the dry linear peptide. The final yield of the unlabelled peptide was 20 dry mg (overall yield 11%) and the fluorescently labelled peptide was 8 mg (yield 2%).

Conditions and Procedures for Capillary Electrophoresis

CE experiments were carried out on a Beckman Coulter ProteomeLab PA800 (Beckman Coulter Inc., Fullerton, CA) instrument with a laser induced fluorescence (LIF) detector (488 nm excitation and 520 nm emission). Uncoated fused-silica capillaries were used for analysis throughout (50 cm total length, 42 cm length to detector, 50 μm inner diameter, 360 μm outer diameter) (Polymicro Technologies, Phoenix, AZ). Prior to use, the capillary was rinsed with 1 M NaOH (30 min), MeOH (30 min), purified water (30 min), and finally the background electrolyte (BGE) (30 min), and was conditioned overnight. At the beginning of each day and between each run, the capillary was rinsed with 0.1 M NaOH (5 min), followed by MeOH (5 min), and water (5 min) and then with corresponding BGE (5 min).

A voltage of +10 kV was then applied across the capillary and the fluorescence signals were recorded. The peptide was injected into a capillary filled with the BGE under a pressure of 0.5 psi (3,447 Pa) for 5 s, and then a voltage of +10 kV was applied when both inlet and outlet vials contained the BGE.

Cell Culture

HUVEC seed cells, media and supplements were obtained from Cascade Biologics (Portland, OR). All other cell culture supplies were obtained from Invitrogen, (Carlesbad, CA). HUVECs were grown in Med200 supplemented with 10% (v/v) Low Serum Growth Supplement. M21 and M21L melanoma cell lines (M21L cells do not express the α_v component of the $\alpha_v\beta_3$ heterodimer, a kind gift from Dr. D. Cheresh) were maintained in 1640 RMPI medium with 10% fetal bovine serum (FBS), in an atmosphere containing 5% CO_2. Cells were grown to confluence yielding approximately 1.0×10^6 cells per 75 cm^2 tissue culture flask for HUVEC and 1.8×10^6 cells/flask for

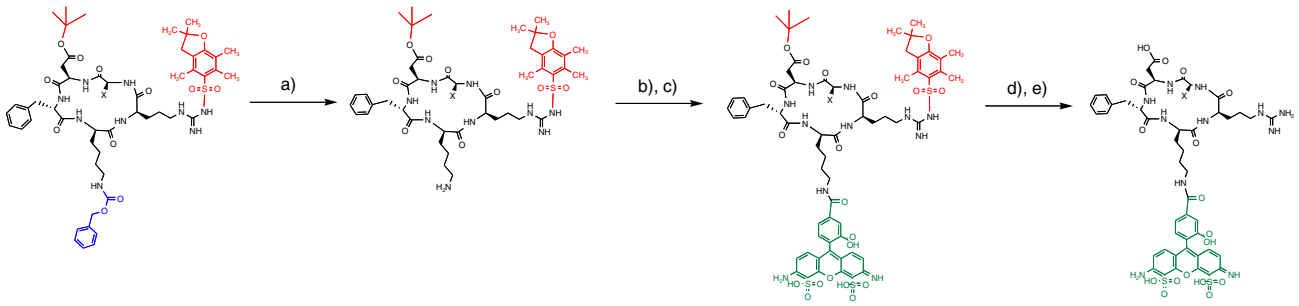

Scheme 1 Synthesis of fluorescnetly labelled ligands. Cyclised and protected peptides were selectively deprotected at lysine ε-amines, and labeled with Alexa Fluor-488. **a** H_2/Pd, **b** Alexa Fluor-488-TFP, TEA, **c** RP-HPLC, **d** 95% TFA, 2.5% H_2O, 2.5% TIS, **e** 2 X RP-HPLC. For cRGDfK-488, X=H and for cRADfK-488, X=CH_3

melanoma cell lines. At the time of harvest, media was removed and cells were rinsed twice with 10 ml phosphate buffered saline (PBS) (with Ca^{2+} and Mg^{2+} present). Adhered cells (HUVEC and M21) were harvested manually with a cell scraper to preserve the integrity of the integrins. Unadhered cell suspensions were washed then centrifuged at 1,100 rpm for 5 min and resuspended in 5% FBS in PBS (herein referred to as PBS/FBS) to a final volume that contained 500,000 cells/ml.

Cell Binding and Uptake

Harvested cells were aliquoted in 200 µl volumes containing approximately 100,000 cells. An antibody saturation curve, Fig. 2b, was made by adding 0–14 nM (in PBS/FBS) of the Alexa Fluor 488-labelled LM609X antibody, which is specific for the $\alpha_v\beta_3$ integrin (Chemicon International, Temecula, CA, USA) to the cells. The Alexa Fluor labelled peptides were quantitated using a standard curve produced from the fluorescence emission at 520 nm following excitation at 495 nm. Once accurately prepared, solutions of the peptides were added to cells over a final concentration range of 0–5 µM. The final volume was adjusted to 500 µl with PBS/FBS. For the kinetic binding experiments shown in Fig. 5, the peptides were added to cells at a concentration of 13.5 µM. Each data point was determined in triplicate. Ligands and cells were incubated at either 37 or 4°C for 1 h for equilibrium binding experiments and 0, 1, 5, 15, 30, 60 and 90 min incubation times for the kinetic binding study. Unbound ligands were removed by rinsing with 5 ml of FACS rinsing buffer (130 mM NaCl, 3 mM KCl, 10.4 mM Na_2PO_4, 1.7 mM KH_2PO_4), followed by centrifugation at 1,100 rpm for 5 min, and repeated twice. Unfixed cells were kept on ice and immediately analyzed by flow cytometry on a BD LSR II flow cytometer equipped with an air–cooled argon-ion laser. The instrument was calibrated weekly for fluorescence and light scattering with 2 µM Calbrite beads. Light scattering and fluorescence channels were set to a logarithmic scale and 10,000 events were collected per sample. Data was analyzed with the program "Flow Joe" (Version 4.5.9, Stanford, CA). Electronic gates were established on unstained live cells based on their ability to exclude the uptake of propidium iodide. The mean fluorescent intensity (MFI) was plotted versus the concentration of peptide and fit to non-linear regression curves using Sigma Plot software from Jandel Scientific (Version 10.1, San Rafael, CA).

Receptor Quantitation

The amount of cell-bound antibody (and thus the number of $\alpha_v\beta_3$ integrins) was determined using a Quantum Simply Cellular kit for antigen quantitation (Bang Laboratories, Cat. No.815A, Fishers, IN). The kit contains microspheres with a series of known amounts of IgG antibody binding sites. A standard curve was constructed by measurement of the signal that the labeled antibody, LM609X, emits when bound to the microspheres (see Fig. 2a). LM609X was added to each series of microspheres in triplicate, and incubated at 4°C for 1 h. The actual amount of antibody used (2 µg) was higher than the manufacturer's recommended value to ensure sufficient saturation of the binding sites on the microspheres. After binding, the excess antibody was removed by washing with 5 ml of FACS rinsing buffer, centrifuging at 1,500 rpm, and repeated twice and the fluorescent signal that was measured was used to construct the standard curve shown in Fig. 2a. The antibody was added to HUVECs, M21 and M21L over a concentration range between 0 and 14 nM and unbound ligands were removed as described above. The number of $\alpha_v\beta_3$ receptors could then be calculated from the maximum level of cell-associated fluorescence (B_{max}) by using the standard curve.

Microscopy

HUVECs were grown to confluence on eight-chambered, glass slides (BD, Franklin Lakes, NJ). Cells were rinsed three times with PBS/FBS and ligands were together with 50 µg of rhodamine-conjugated dextran, a fluid-phase endocytosis marker, (Molecular Probes, Eugene, OR) as follows: 13.5 µM of cRGDfK-488 or cRADfK-488 (4 µg) in PBS/FBS, at a total volume of 200 µl, 1 µg of LM609X in 200 µl of PBS/FBS and, for comparison, a treatment control of 200 µl of PBS/FBS. Each slide was incubated at either 4 or 37°C for 15 min and 1 h. Ligands were removed by washing each slide three times with PBS/FBS then fixed with 3.5% paraformaldehyde in PBS for 15 min. Immediately before imaging, chambers were removed, and the slides were prepared using Vectashield mounting media (Vector Laboratories, Burlingame, CA) containing the blue nuclear stain, 4′,6-diamidino-2-phenylindole (DAPI). Cells were visualized on a Zeiss Axiovert 200 fluorescence microscope equipped with a Retiga 2000R camera. Images were captured under a bright field with a 0.3 s exposure time. In the fluorescent fields, the exposure times were: red-3.1 s, green-8.1 s, and blue-0.005 s for each image. Images were compiled using Openlab software (Version 5.0, Improvision, Lexington, MA).

Results and Discussion

Peptide Characterization

Particular attention was paid to achieving the maximum purity of labeled peptides. The water-soluble compound,

cRGDfK-488 was inherently difficult to separate from the reactants and careful purification and analysis steps were required to ensure low levels of contamination before biological evaluation. CE proved to be a convenient method for analyzing the purity of the peptide-conjugated fluorochrome, which was poorly resolved by analytical HPLC or various TLC methods. The cRGDfK-488 conjugate was characterized by an electrophoretic mobility, which is determined by the charge to size ratio of the molecule. A typical electrophoregram demonstrating the purity of the cRGDfK-488 conjugate is shown in Fig. 1. Advanced analytical techniques, such as CE separation, are necessary for the accurate qualification of peptides that contain a water-soluble label.

Number of $\alpha_v\beta_3$ Integrins per Cell

Before the binding of cRGDfK-488 to $\alpha_v\beta_3$ integrin receptors on HUVECs was studied, it was important to establish that the HUVECs express high levels of the $\alpha_v\beta_3$ integrin. The number of receptors was thus assayed by incubating the cells with saturating levels of the Alexa Fluor-488-conjugated antibody, LM609X, which is specific for $\alpha_v\beta_3$. The amount of cell-bound antibody was quantitated using a standard curve produced from saturation of antibody binding microspheres as detailed in Methods. The mean fluorescent intensity (MFI) of the microspheres increases linearly with the number of antibody binding sites that are engineered on the particle (Fig. 2a). The maximum MFI values resulting from a saturation curve of LM609X binding to HUVEC, or M21L cell lines (shown in Fig. 2b) were used to interpolate the number of integrins/cell from the standard curve produced in Fig. 2a.

Using this method, HUVECs were determined to have $(2.63 \pm 0.08) \times 10^5$ $\alpha_v\beta_3$ integrins per cell, in reasonable agreement with previous estimates of $(4.2 \pm 1.6) \times 10^5$ integrins per HUVEC (Smith and Giorgio 2004). The results from these assays showed that M21L cells had $(1.4 \pm 0.6) \times 10^3$ integrins per cell. To gain perspective on published RGD-internalization studies using M21 melanoma cells (Castel et al. 2001), this cell line was also measured and found to express $(5.6 \pm 0.3) \times 10^4$ integrins per cell. The measured K_d value for LM609X binding to HUVEC in this experiment was 14.4 nM.

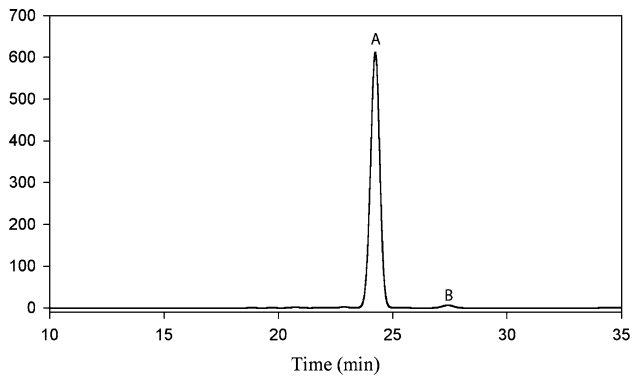

Fig. 1 A typical electrophoregram for cRGDfK-488, demonstrating the high level of purity [i.e. >98%; ([A]/[A] + [B])] that was obtained for the peptide ligands. This level of purity was made possible by additional HPLC purification steps, which were found to be necessary in order to resolve the labelled peptide (**a**) from the unconjugated fluorophore (**b**)

cRGDfK-488 Binds to Cellular $\alpha_v\beta_3$ Integrin and is Subsequently Endocytosed

Binding by the Alexa Fluor-labelled peptides is illustrated in Fig. 3a, where the non-specific binding to HUVEC of cRADfK-488 (cRADfK does not contribute to $\alpha_v\beta_3$ integrin antagonism Pfaff et al. 1994) is shown to increase linearly while the total binding of cRGDfK-488 produces a hyperbolic curve. Figure 3b shows a similar trend when M21L cells, which do not have a functional α-subunit (Cheresh and Spiro 1987), are used.

Previous studies employing M21 and M21L cells (Castel et al. 2001) have suggested that cRGDfK ligands are accumulated into cells via an integrin-independent fluid phase endocytosis mechanism, and that the cell-associated ligand is independent of the presence of integrin on the cell membrane. In order to investigate the influence of integrin density on cell-associated ligands, the binding of cRGDfK-488 to M21L cells, which exhibit much lower levels of integrin expression than HUVECs, was investigated. As shown in Fig. 3, the HUVEC cells incorporate a much larger concentration of cRGDfK-488 compared to the M21L cells. Additionally, the non-specific binding, as measured by the uptake of cRADfK-488, contributes a larger proportion of the total binding for M21L cells, compared to HUVEC cells in Fig. 3a. This is consistent with the requirement for expression of $\alpha_v\beta_3$ for association of cRGDfK-488 to cells. It is important to note that the levels of binding observed for the cRGDfK-488 ligands are not significantly larger than observed for background binding as assayed by the cRADfK-488 ligand, suggesting that specific binding may well be obscured by non-specific effects for cells with low densities of integrin receptors.

The saturation curves shown in Fig. 3 describe peptides that are bound to surface integrins and the peptides that are endocytosed. In order to investigate the influence of endocytosis on binding, the association of peptides with HUVEC following 1 h incubations at 4°C (endocytosis inhibiting) and 37°C (endocytosis permitting) was investigated.

Using the specific binding curves produced at endocytosis inhibiting temperatures, an apparent dissociation constant, K_d, for cRGDfK-488 binding to cellular $\alpha_v\beta_3$ was determined to be 0.20 μM ± 0.04. As shown in Fig. 4a, a marked

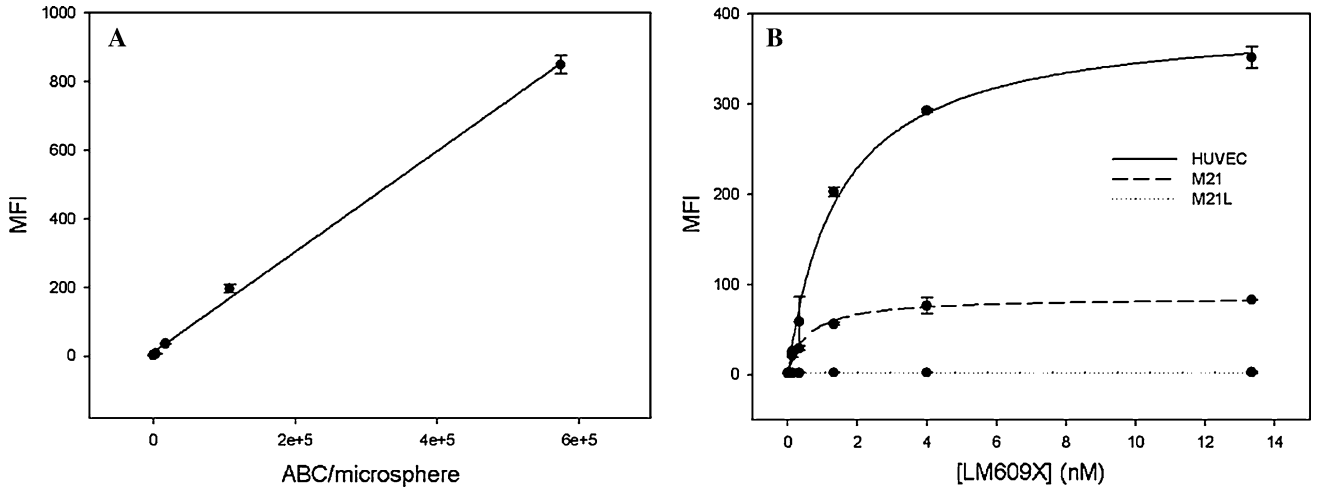

Fig. 2 Quantitation of $\alpha_v\beta_3$ integrin expression on the cell surface **a** *Standard curve* for antibody-induced-fluorescence (MFI) of calibrated microspheres that have a known antibody binding capacity (ABC). The best fit to this data was for the linear equation $y = 11.889 + (0.002)x$. MFI is a measure of the mean fluorescence intensity (*arbitrary units*) detected by a flow cytometry (cytometer with $n = 3$). ± SD. **b** *Regression curves* generated by titrating the antibody to achieve saturation of the $\alpha_v\beta_3$ receptor on HUVEC (*solid curve*) M21 melanoma cells (*medium dashed curve*) and M21L melanoma cells (*dotted curve*), with the fluorescently labeled antibody LM609X. The maximum number of binding sites (B_{max}) and standard error values were calculated by fitting the saturation curves to the equation $y = B_{max}(x)/(K_d + x)$. B_{max} was then used to determine the average number of receptors for each cell line as indicated in the text ± the standard error

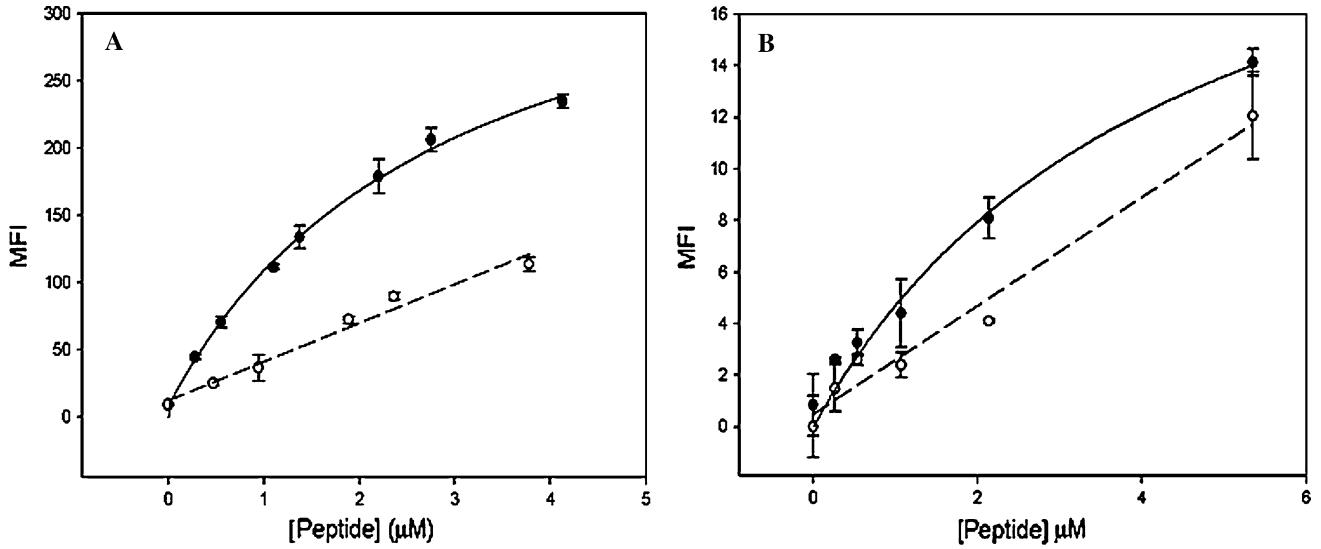

Fig. 3 Binding isotherms for the fluorescently labeled RGD and RAD peptides to HUVEC or M21L cells following 1 h incubations with the peptide ligands at 37°C. **a** Saturation curves characterizing the binding of cRGDfK-488 (*closed circles*) and cRADfK-488 (*open circles*) to HUVEC (live cell population) as measured by mean fluorescence intensity following incubation at the peptide concentrations indicated. **b** Saturation curves describing the binding of Alexa-Fluor 488 labeled RGD (*closed circles*) and RAD (*open circles*) peptides to M21L cells that express low levels of the $\alpha_v\beta_3$ integrin. Measurements were done in triplicate with *error bars* representing the standard deviation

difference in the specific binding of cRGDfK-488 between 4 and 37°C was observed, corresponding to a 7.4-fold increase in the measured B_{max}. In contrast, binding of the antibody (LM609X) is only moderately elevated (1.9-fold) when endocytosis is permitted, as shown in Fig. 4b. Similarly, M21L cells that express low levels of the $\alpha_v\beta_3$ integrin exhibit a modest 2.8-fold increase in the measured binding (Fig. 4c).

In order to further characterize the increased cell-associated fluorescence observed at endocytosis permitting temperatures, a kinetic study of peptide binding to HUVECs at both 4 and 37°C was performed. The time-dependent binding of cRGDfK-488 and of the control peptide (cRADfK-488) to HUVEC over 2 h is illustrated in Fig. 5. It is observed that saturation occurs more rapidly at 4°C than at

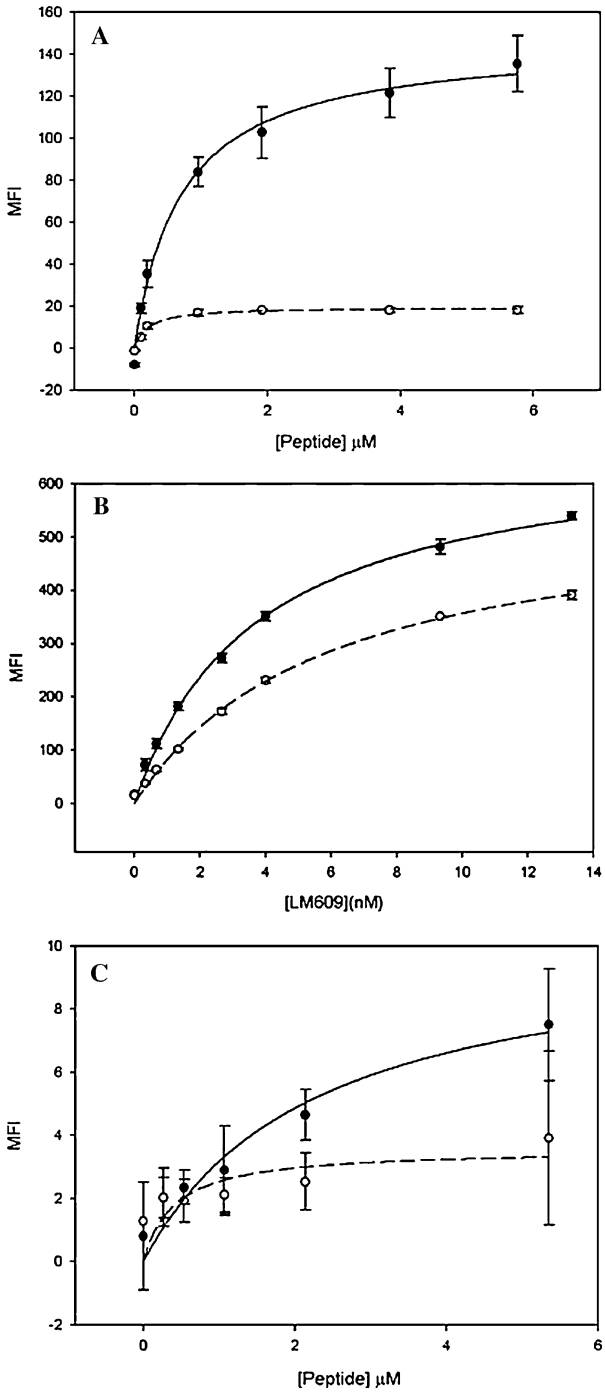

Fig. 4 Binding of cRGDfK-488 and LM609 to HUVEC and M21 cells at endocytosis permitting and endocytosis inhibiting temperatures. Saturation curves describing the binding of RGD peptide and mAb to HUVEC following a 1 h incubation at endocytosis enabling (37°C, *closed circles*) and endocytosis inhibiting (4°C, *open circles*) temperatures. **a** Specific binding (total binding minus non-specific binding, as assayed employing the RAD peptide) of cRGDfK-488 to HUVEC. **b** Specific binding of the antibody, LM609X, to HUVEC **c** Specific binding of cRGDfK-488 to M21L cells, which do not express the full $\alpha_v\beta_3$ integrin on their surface. *Error bars* were calculated from the square root of the sum of squares of the error from non-specific binding and total binding

37°C due to the fact that binding at low temperatures is limited to a finite number of integrin sites on the cell surface. However, at 37°C the saturation point is still not reached after 2 h. This may be explained by the fact that, in receptor-mediated endocytosis, integrins become temporarily unavailable as they chaperone ligands into the cell, but then reappear at the surface following dissociation of the ligand.

As the amount of receptor on the surface of cells is very low compared to the amount of the ligand in solution, a first-order kinetic analysis was applied to the time-course data in order to estimate the rate constants, k_{obs}, listed in Table 1. Because of the many systematic changes that accompany a decrease in temperature, including reduced solubility of ligands and reduced rates of diffusion, it is difficult to interpret the rate constants individually. Instead it is simpler to consider the rate of cRGDfK-488 relative to the rate of cRADfK-488. At endocytosis inhibiting temperatures the ratio, R, is 0.26, indicating that the control peptide, cRADfK-488, is binding to the cell surface more quickly than cRGDfK-488. However, at endocytosis permitting temperatures, $R = 1.75$, suggesting that there is a different mechanism in place which is preferential towards the uptake of cRGDfK-488. These findings support the hypothesis of receptor-mediated endocytosis as the primary mechanism for the uptake of cRGDfK-488. In order to evaluate this more definitively, fluorescence microscopy studies were undertaken.

Endocytosis as Visualized by Fluorescence Microscopy

In order to lend support to the notion that HUVECs endocytose the cRGDfK-488 ligands at permissive temperatures, uptake was followed by fluorescence microscopy. Images of cells following either 15 min or 1 h incubations at 37°C are shown in Fig. 6. Similar to cells in suspension, as analyzed by flow-cytometry, the ligand cRGDfK-488 appears to be rapidly endocytosed. Co-localization of the green peptide label with the red endocytosis marker (rhodamine-conjugated dextran) commenced as early as 15 min and within 1 h, the two labels overlap. Internalization of the LM609X antibody was weakly visible, consistent with the modest increase in B_{max} with temperature, observed for LM609X binding to suspended HUVEC (Fig. 4a). It is important to note that the cRGDfK-488 peptide induced unique morphological changes (seen best in the bright field images) that are different from those seen for LM609X or cRADfK-488 treated cells. In particular, the cells lost their adhesive properties and detached from the glass surface. Few cells remained adhered to the glass slide after cRGDfK-488 was removed by the required washing steps (Fig. 7).

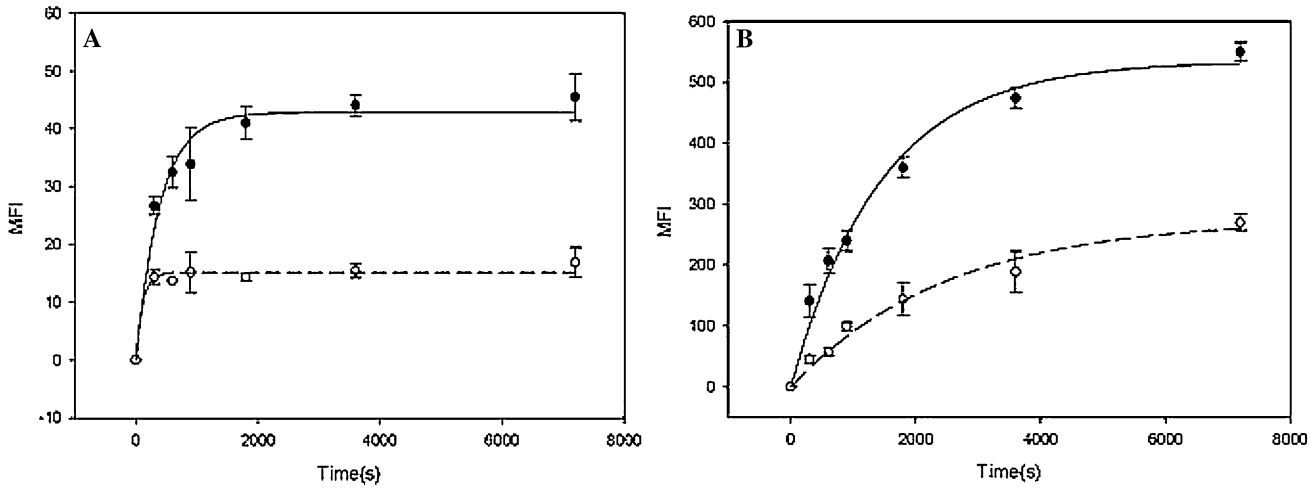

Fig. 5 Uptake of labelled peptides by HUVEC. Cells were incubated with 13.5 μM cRGDfK-488 (*closed circles*) or cRADfK-488 (*open circles*) at **a** Endocytosis inhibiting (4°C) and **b** Endocytosis permitting (37°C) temperatures. The *curves* represent the best fit of the data to the first order rate equation, $y(t) = a\left(1 - e^{-k_{obs}t}\right)$

Table 1 Estimated kinetic parameters for the uptake of labeled peptides by HUVEC under endocytosis inhibiting (4°C) and permitting (37°C) conditions

Temperature [°C]	cRGDfK-488		cRADfK-488		$R = \left(\frac{k_{obs,\,RGD}}{k_{obs,\,RAD}}\right)$
	k_{obs} (s^{-1})	$t_{1/2}$ (s)	k_{obs} (s^{-1})	$t_{1/2}$ (s)	
4	0.0024	288	0.009	77	0.26
37	0.0007	1,004	0.0004	1,732	1.75

The same ligand incubations were carried out at 4°C with less overall binding detected for all ligands and most cells remain adhered to the glass slide. LM609X and to a lesser degree, cRGDfK-488, can be seen at the periphery of the cell after 1 h.

Relative Findings

The major finding of this work is that the cRGDfK-488 peptide binds to $\alpha_v\beta_3$ integrins on HUVECs and stimulates endocytosis when compared to the LM609X monoclonal antibody or the cRADfK-488 negative control. There are three interesting aspects of this observation. First, it is of interest to compare the ability of the RGD-containing ligand used here to stimulate endocytosis following binding to the $\alpha_v\beta_3$ integrin with the properties of RGD-containing ligands reported by other investigators. The second area concerns the mechanism by which the peptide ligand could stimulate greater endocytosis than other ligands such as the monoclonal antibody. The final point concerns the potential utility of the cRGDfK-488 peptide as a useful agent to target drugs in vivo.

The relation between RGD peptide binding to integrins and subsequent uptake into cells is a subject of much interest. For melanoma cells, it has been reported that mAb binding to integrins results in receptor mediated endocytosis, whereas cRGDfK is taken up by an integrin independent process (Castel et al. 2001). The conclusion that cRGDfK is taken up by an integrin independent process was indicated by similar levels of uptake for ^{3}H-cRGDfK and carboxyfluorescein (CF) labeled cRGDfK for both M21 and M21L cells at both 4 and 37°C. These results are not in agreement with the results presented here, because little specific binding (and much reduced uptake) of the cRGDfK-488 peptide is observed for the M21L cell line that expresses low levels of receptors. Further, uptake of the cRADfK-488 control peptide, which binds non-specifically to the HUVEC, is considerably reduced compared to the cRGDfK-488 ligand (Fig. 3a). The RGD ligands employed in this study were designed to be soluble in an aqueous environment to reduce background binding and are highly purified as demonstrated by CE and mass spectrometry analyses. Two effects may clarify discrepancies in the literature. First, HUVECs express nearly 200 times more integrin receptors than M21L cells, whereas the M21 cells have only 40 times higher levels of receptors as compared to M21L cells. In our experience, specific binding facilitates endocytosis and for cells that express a very high level of the receptor, endocytosis is more significant. A second and related point is that the use of ligands with higher non-specific background binding properties can lead to additional difficulties in detecting integrin-specific effects. In the previous study the binding and uptake properties of RAD control ligands were not examined. Other studies demonstrating enhanced gene delivery of vectors targeted by RGD ligands support a specific receptor-mediated endocytotic process (Renigunta et al. 2006). Specific uptake of RGD-containing ligands is

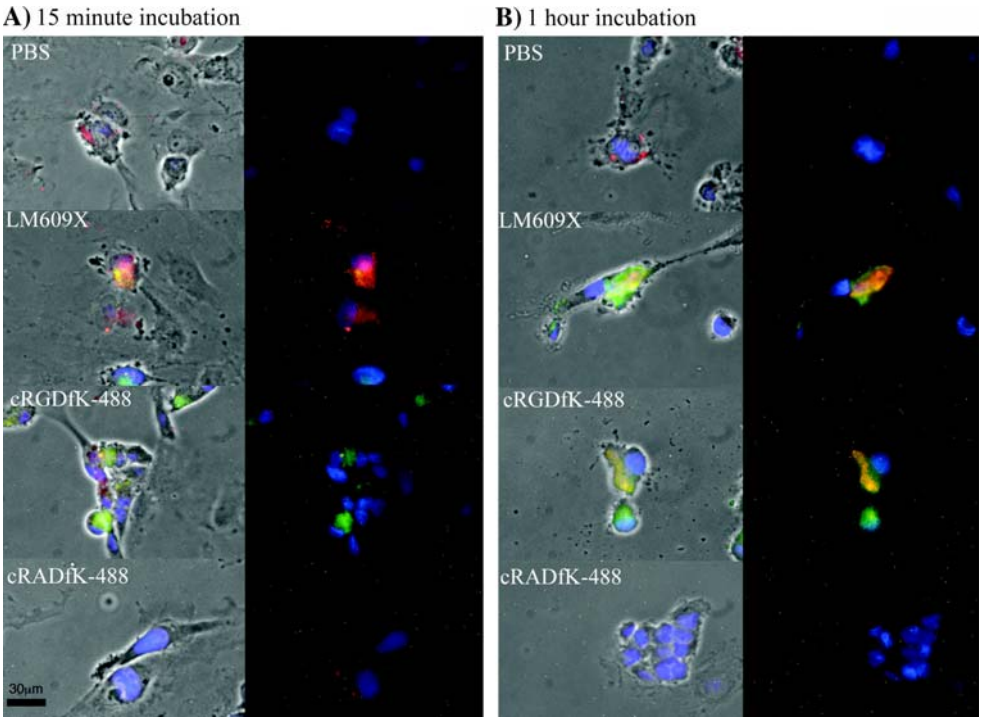

Fig. 6 Fluorescence microscopy of HUVEC following incubation with the LM609X mAb, cRGDfK-488 and cRADfK-488 ligands at 37°C. The Alexa Fluor 488 labeled ligands were added together with dextran rhodamine to visualize endocytosis. Fluorescence micrographs obtained **a** Following a 15 min incubation and **b** Following a 1 h incubation. The data indicates that cRGDfK-488 co-localizes with endcytosed vesicles while LM609X is largely visible at the surface of the cell. Non-specific binding by cRADfK-488 was not detected

also supported by studies indicating that RGD internalization coincides with the activation of a kinase (S6K1) that is critical for cell growth. This effect is RGD specific since the negative control (an RGE-containing peptide) is neither internalized nor active in S6K1 phosphorylation (Balasubramanian and Kuppuswamy 2003).

The next area of discussion concerns the mechanism whereby the cRGDfK-488 ligand could stimulate appreciably higher levels of internalization on binding to the $\alpha_v\beta_3$ integrin as compared to the integrin-specific mAb, LM609X. A number of studies suggest that the interactions of RGD ligands with integrins have significantly different features than binding of mAb. A two-step process has been proposed for fluorescently labeled RGD-peptides that bind to the main integrin on activated platelets, GPIIb/IIIa. In this study, a rearrangement process was proposed to follow the initial binding event (Bednar et al. 1997). The ratio of k_{off}/k_{on} for the first step was observed to be high compared to the second step, indicating that the subsequent rearrangement stabilizes a complex that is less prone to dissociation. Capillary electrophoresis studies on the binding of the cRGDfK-488 ligand to isolated $\alpha_v\beta_3$ integrins indicate that two binding sites for the RGD ligand exist on the receptor. However, the second binding event seems to have a similar affinity compared to the first one (Sun et al. 2007). While it is not clear how these different binding characteristics of the RGD ligand as compared to the mAb lead to enhanced endocytosis for the RGD ligand, it is clear that the possibility exists for substantially different conformational and functional consequences for RGD binding as compared to mAb binding. It will be of interest to pursue the correlation between these differences and subsequent endocytotic events.

The use of RGD-containing peptides for the targeted delivery of associated therapeutics is clearly improved by an enhanced probability of endocytosis. A related question concerns whether the specific type of RGD peptide influences the levels of endocytosis or whether RGD ligands have the same endocytotic index. In this study, the AlexaFluor-488 cargo was highly soluble in water and had a similar molecular weight to that of the RGD targeting peptide. This condition may improve the chances that RGD peptides will carry fluorescent labels into cells. It will be of additional interest to examine the endocytotic index of multivalent RGD targeting ligands, which demonstrate improved binding to the $\alpha_v\beta_3$ integrins (Montet et al. 2006a).

Concluding Remarks

The results presented in this study established that cRGDfK-488 stimulates enhanced endocytosis in HUVECs as compared to the mAb LM609X, and that the uptake of the RGD ligand proceeds via an endocytotic process that involves RGD-specific interactions with cells that express a very high level of the $\alpha_v\beta_3$ integrin. It is anticipated that for RGD-targeted therapeutics the maximum therapeutic benefit will result from the use of targeting ligands that maximize intracellular delivery of associated cargo,

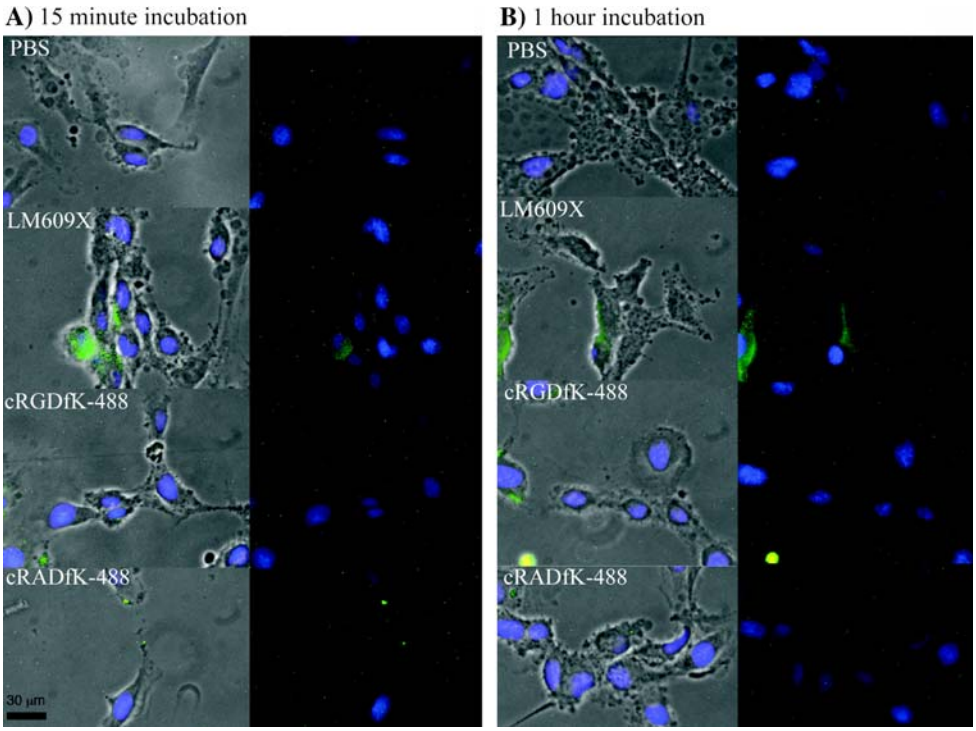

Fig. 7 Fluorescence microscopy of HUVEC following incubation with the LM609XmAb, cRGDfK-488 and cRADfK-488 ligands at 4°C. The Alexa Fluor 488 labeledligands were added together with dextran rhodamine to visualize endocytosis. Imageswere obtained **a** following a 15 min incubation and **b** following a 1 h incubation. Only antibody binding can be detected at the surface of the cell

pointing out a need to characterize targeting peptides according to their relative ability to stimulate endocytosis in target cells.

Acknowledgments We thank Dr. David Cheresh for the melanoma cell lines, Dr. Mark Okon for NMR expertise, Dr. Scott Covey for assistance with microscopy and Mr. Ian T. Dobson for his technical assistance. This work was supported by grants from the Canadian Institute for Health Research, the Natural Sciences and Engineering Research Council of Canada and Tekmira Pharmaceuticals Inc. S.C. and E.J.M. are funded by Natural Sciences and Engineering Research Council of Canada Postgraduate Scholarships.

References

Albelda SM, Mette SA, Elder DE, Stewart R, Damjanovich L, Herlyn M, Buck CA (1990) Integrin distribution in malignant melanoma: association of the beta 3 subunit with tumor progression. Cancer Res 50:6757–6764

Albert JM, Cao C, Geng L, Leavitt L, Hallahan DE, Lu B (2006) Integrin alpha v beta 3 antagonist Cilengitide enhances efficacy of radiotherapy in endothelial cell and non-small-cell lung cancer models. Int J Radiat Oncol Biol Phys 65:1536–1543

Arap W, Pasqualini R, Ruoslahti E (1998) Cancer treatment by targeted drug delivery to tumor vasculature in a mouse model. Science 279:377–380

Balasubramanian S, Kuppuswamy D (2003) RGD-containing peptides activate S6K1 through beta3 integrin in adult cardiac muscle cells. J Biol Chem 278:42214–42224

Bednar B, Cunningham ME, Mcqueney PA, Egbertson MS, Askew BC, Rednar R, Hartman GD, Gould RJ (1997) Flow cytometric measurement of kinetic and equilibrium binding parameters of Arginine-Glycine-Aspartic acid ligands in binding to glycoprotein IIb/IIIa on platelets. Cytometry 28:58–65

Beer AJ, Haubner R, Sarbia M, Goebel M, Luderschmidt S, Grosu AL, Schnell O, Niemeyer M, Kessler H, Wester HJ, Weber WA, Schwaiger M (2006) Positron emission tomography using [18F]Galacto-RGD identifies the level of integrin alpha(v)beta3 expression in man. Clin Cancer Res 12:3942–3949

Brassard DL, Maxwell E, Malkowski M, Nagabhushan TL, Kumar CC, Armstrong L (1999) Integrin alpha(v)beta(3)-mediated activation of apoptosis. Exp Cell Res 251:33–45

Brooks PC, Clark RAF, Cheresh DA (1994) Requirement of vascular integrin, avB3 for angiogenesis. Science 264:569–571

Burkhart DJ, Kalet BT, Coleman MP, Post GC, Koch TH (2004) Doxorubicin-formaldehyde conjugates targeting alphavbeta3 integrin. Mol Cancer Ther 3:1593–1604

Castel S, Pagan R, Mitjans F, Piulats J, Goodman S, Jonczyk A, Huber F, Vilaro S, Reina M (2001) RGD peptides and monoclonal antibodies, antagonists of alpha(v)-integrin, enter the cells by independent endocytic pathways. Lab Invest 81:1615–1626

Chen X, Plasencia C, Hou Y, Neamati N (2005) Synthesis and biological evaluation of dimeric RGD peptide-paclitaxel conjugate as a model for integrin-targeted drug delivery. J Med Chem 48:1098–1106

Cheresh DA, Spiro RC (1987) Biosynthetic and functional properties of an Arg-Gly-Asp-directed receptor involved in human melanoma cell attachment to vitronectin, fibrinogen, and von Willebrand factor. J Biol Chem 262:17703–17711

Dechantsreiter MA, Planker E, Matha B, Lohof E, Holzemann G, Jonczyk A, Goodman SL, Kessler H (1999) *N*-Methylated cyclic RGD peptides as highly active and selective alpha(V)beta(3) integrin antagonists. J Med Chem 42:3033–3040

Dubey PK, Mishra V, Jain S, Mahor S, Vyas SP (2004) Liposomes modified with cyclic RGD peptide for tumor targeting. J Drug Target 12:257–264

Folkman J (1990) What is the evidence that tumors are angiogenesis dependent? J Natl Cancer Inst 82:4–6

Gladson CL, Cheresh DA (1991) Glioblastoma expression of vitronectin and the alpha v beta 3 integrin. Adhesion mechanism for transformed glial cells. J Clin Invest 88:1924–1932

Haubner R, Gratias R, Diefenbach B, Goodman SL, Jonczyk A, Kessler H (1996) Structural and functional aspects of RGD-containing cyclic pentapeptides as highly potent and selective integrin avB3 antagonists. J Am Chem Soc 118:7461–7472

Hieken TJ, Farolan M, Ronan SG, Shilkaitis A, Wild L, Das Gupta TK (1996) Beta3 integrin expression in melanoma predicts subsequent metastasis. J Surg Res 63:169–173

Kim JW, Lee HS (2004) Tumor targeting by doxorubicin-RGD–4C peptide conjugate in an orthotopic mouse hepatoma model. Int J Mol Med 14:529–535

Liapis H, Adler LM, Wick MR, Rader JS (1997) Expression of alpha(v)beta3 integrin is less frequent in ovarian epithelial tumors of low malignant potential in contrast to ovarian carcinomas. Hum Pathol 28:443–449

Montet X, Funovics M, Montet-Abou K, Weissleder R, Josephson L (2006a) Multivalent effects of RGD peptides obtained by nanoparticle display. J Med Chem 49:6087–6093

Montet X, Montet-Abou K, Reynolds F, Weissleder R, Josephson L (2006b) Nanoparticle imaging of integrins on tumor cells. Neoplasia 8:214–222

Pfaff M, Tangemann K, Muller B, Gurrath M, Muller G, Kessler H, Timpl R, Engel J (1994) Selective recognition of cyclic RGD peptides of NMR defined conformation by alpha IIb beta 3, alpha V beta 3, and alpha 5 beta 1 integrins. J Biol Chem 269:20233–20238

Puklin-Faucher E, Gao M, Schulten K, Vogel V (2006) How the headpiece hinge angle is opened: new insights into the dynamics of integrin activation. J Cell Biol 175:349–360

Renigunta A, Krasteva G, Konig P, Rose F, Klepetko W, Grimminger F, Seeger W, Hanze J (2006) DNA transfer into human lung cells is improved with Tat-RGD peptide by caveoli-mediated endocytosis. Bioconjug Chem 17:327–334

Ruoslahti E, Pierschbacher MD (1987) New perspectives in cell adhesion: RGD and integrins. Science 238:491–497

Schiffelers RM, Koning GA, Ten Hagen TL, Fens MH, Schraa AJ, Janssen AP, Kok RJ, Molema G, Storm G (2003) Anti-tumor efficacy of tumor vasculature-targeted liposomal doxorubicin. J Control Release 91:115–122

Schraa AJ, Kok RJ, Botter SM, Withoff S, Meijer DK, De Leij LF, Molema G (2004) RGD-modified anti-CD3 antibodies redirect cytolytic capacity of cytotoxic T lymphocytes toward alphavbeta3-expressing endothelial cells. Int J Cancer 112:279–285

Smith RA, Giorgio TD (2004) Quantitation and kinetics of CD51 surface receptor expression: implications for targeted delivery. Ann Biomed Eng 32:635–644

Storgard CM, Stupack DG, Jonczyk A, Goodman SL, Fox RI, Cheresh DA (1999) Decreased angiogenesis and arthritic disease in rabbits treated with an alphavbeta3 antagonist. J Clin Invest 103:47–54

Sun Y, Cressman S, Fang N, Cullis PR, Chen DDY (2007) Capillary electrophoresis frontal analysis for characterization of avb3 integrin binding interactions. Anal Chem 80:3105–3111

Von Wallbrunn A, Holtke C, Zuhlsdorf M, Heindel W, Schafers M, Bremer C (2006) In vivo imaging of integrin alphanubeta(3) expression using fluorescence-mediated tomography. Eur J Nucl Med Mol Imaging 34:745–754

Wu Y, Zhang X, Xiong Z, Cheng Z, Fisher DR, Liu S, Gambhir SS, Chen X (2005) microPET imaging of glioma integrin {alpha}v{-beta}3 expression using (64)Cu-labeled tetrameric RGD peptide. J Nucl Med 46:1707–1718

Xiong XB, Huang Y, Lu WL, Zhang X, Zhang H, Nagai T, Zhang Q (2005) Intracellular delivery of doxorubicin with RGD-modified sterically stabilized liposomes for an improved antitumor efficacy: in vitro and in vivo. J Pharm Sci 94:1782–1793